ORIGINAL ARTICLE

Silencing of RAD51AP1 suppresses epithelial–mesenchymal transition and metastasis in non-small cell lung cancer

Yuanyuan Wu[1†], Huifeng Wang[1†], Lijiao Qiao[2], Xiangming Jin[1], Hui Dong[3] ⬤ & Yan Wang[1]

1 Department of Oncology, Cancer Hospital, General Hospital of Ningxia Medical University, Yinchuan, China
2 Department of Oncology, Cancer Hospital, General Hospital of Ningxia Medical University, Yinchuan, China
3 Center of Research Equipment Management, General Hospital of Ningxia Medical University, Yinchuan, China

Abstract

Background: Non-small cell lung cancer (NSCLC) is a major cause of cancer-related mortality and is frequently accompanied by metastasis. The crucial roles of genes in lung cancer have attracted attention. Thus, this study aimed to investigate the effects of RAD51AP1 on the epithelial–mesenchymal transition (EMT) and metastasis of NSCLC.

Methods: The positive expression rate of the RAD51AP1 protein was examined. NSCLC cells were transfected with a series of plasmids to alter the expression of RAD51AP1 to clarify the influence of RAD51AP1 on EMT and metastasis in NSCLC, as well as NSCLC cell migration, invasion, apoptosis, proliferation, and cloning. An in vivo experiment was conducted to determine the oncogenicity of human NSCLC cells in nude mice.

Results: RAD51AP1 was highly expressed in NSCLC tissues. Furthermore, we found promotion of N-cadherin, vimentin, fibronectin, MMP-2, OPN, CD62, and TMP-2, but inhibition of E-cadherin, occludin, cytokeratin in the context of elevated RAD51AP1 expression. An in vivo experiment also confirmed that silencing of RAD51AP1 could inhibit NSCLC tumor formation and growth.

Conclusion: Our results revealed that RAD51AP1 silencing suppressed the EMT and metastasis of NSCLC, thereby highlighting its potential as a promising novel target for NSCLC treatment.

Introduction

Lung cancer currently ranks as the leading cause of cancer-related mortality in men and the second leading cause in women throughout the world, with variations in its incidence and trends, including gender, age, and race.[1] Non-small cell lung cancer (NSCLC), presenting primarily as squamous cell carcinoma and non-squamous carcinoma, accounts for approximately 85% of all lung cancer diagnoses.[2] Various intrinsic factors, such as distant metastasis, lymph node metastasis, large tumors, and squamous cell carcinoma, facilitate the poor survival of NSCLC.[3] Epithelial–mesenchymal transition (EMT) is thought to be associated with cancer initiation and leads to the metastasis of cancer cells.[4] Metastasis is a major cause of cancer-related mortality.[5] Furthermore, EMT is reported to participate in drug resistance and metastasis in lung cancer and the inhibition of EMT exerts suppressive effects on lung cancer cell invasion in vitro.[6] Thus, a better understanding of the molecular mechanisms of the EMT and metastasis of NSCLC and an exploration of novel therapeutic and diagnostic targets for NSCLC treatment is required.

A former study highlighted the potential of targeting RAD51 as a new and effective therapeutic strategy for NSCLC.[7] RAD51AP1 is a DNA-binding protein that could stimulate the activity of *RAD51*, which plays an important role in *RAD51*-mediated homologous recombination.[8] Existing literature has revealed that RAD51AP1 is highly expressed in ovarian and lung cancers, and silencing RAD51AP1 has an inhibitory effect on ovarian and lung cancer cell proliferation in vitro through RNA interference.[9] A strong association has been reported between elevated RAD51AP1 and poor prognosis and overall survival of

patients with lung adenocarcinoma.[10] RAD51AP1 is dysregulated in tumor samples and thus may represent a novel marker for hepatitis C virus-mediated hepatocarcinogenesis.[11] Moreover, studies have related the involvement of RAD51AP1 to cell proliferation and DNA repair in intrahepatic cholangiocarcinoma. Silencing of RAD51AP1 contributes to the suppression of cholangiocarcinoma cell growth.[12] Based on the results of these previous studies, we hypothesized that RAD51AP1 may affect NSCLC development. This study was designed to test this hypothesis in order to offer insights into the underlying molecular mechanisms in NSCLC progression, thus providing more effective therapy strategies for NSCLC patients.

Methods

Ethics statement

The Ningxia Medical University General Hospital Scientific Research Ethics Committee approved this study, which was conducted in strict accordance with the Declaration of Helsinki. All participating patients signed written informed consent. All animal experiments were conducted under the approval of the Ningxia Medical University General Hospital Scientific Research Ethics Committee (No. 201805002). Significant measures were taken to minimize animal suffering.

Microarray analysis

The Gene Expression Omnibus (GEO) database (https://www.ncbi.nlm.nih.gov/geo/) was used to retrieve NSCLC-related microarray datasets, from which GSE19188, GSE101929, GSE33532, and GSE74706 were selected and used for the screening of differentially expressed genes (DEGs). Table 1 illustrates the detailed information of microarray datasets. The affy package from R language was adopted for background correction and standardization of microarray data,[13] while the limma package was employed to screen DEGs with a screening threshold of $|log2FolfChange| > 2.0$ and *adj.p.Val* < 0.05.[14] Incorporating this data, the heat maps of DEGs were drawn. Calculate and draw custom Venn diagrams (http://bioinformatics.psb.ugent.be/webtools/Venn/), a tool for online Venn analysis, was employed to compare DEGs in the four microarray datasets. The STRING database (https://string-db.org/) served as a source for information related to protein interaction.[15] Cytoscape 3.6.0 software was used to obtain the interaction information of DEGs.[16] A protein–protein interaction (PPI) network (combined score > 0.4) was then constructed. Finally, the relationship between DEGs and NSCLC was explored via Chilibot (http://www.chilibot.net/

Table 1 Microarray data of NSCLC

Accession	Platform	Organism	Sample
GSE19188	GPL570	*Homo sapiens*	91 NSCLC and 65 adjacent normal lung tissue samples
GSE101929	GPL570	Homo sapiens	32 NSCLC and 34 adjacent normal lung tissues
GSE33532	GPL570	Homo sapiens	80 NSCLC and 20 matched distant normal lung tissues
GSE74706	GPL13497	Homo sapiens	18 tumor-free lung and 18 NSCLC specimens

NSCLC, non-small cell lung cancer.

index.html),[17] after which a relationship network was constructed.

Study subjects

A total of 91 wax block specimens were obtained from patients (56 men, 35 women, aged 25–83 years) who had previously undergone surgical resection for lung cancer at the Department of Pathology, General Hospital of Ningxia Medical University between 2016 and 2017. Adjacent normal lung tissues were taken as controls. None of the patients had been administered chemoradiotherapy before undergoing surgery. Among the 91 NSCLC patients, 49 had lung squamous cell carcinoma, 35 had lung adenocarcinoma, and the remaining seven patients were classified with other types of cancer. There were 38 cases of lymph node metastasis (N2) and 53 cases of non-lymph node metastasis (N0–N1). Fifty-one patients were confirmed at stage I + II and 40 patients at stage III according to the seventh edition 2009 International Association for the Study of Lung Cancer (IASLC) staging criteria. All specimens were surgically resected from hospitalized patients with complete clinical information and follow-up data, and pathologically confirmed as NSCLC. Tissue classification was conducted based on World Health Organization tumor classification criteria.

Immunohistochemistry

Paraffin-embedded specimens were sliced into 4 μm serial sections. Sections were baked at 60°C for one hour, dewaxed using xylene, dehydrated using gradient alcohol, and treated with antigen retrieval under high pressure for 1–3 minutes. Subsequently, 10% normal goat serum blocking solution was added to the sections (Beijing ComWin Biotech Co., Ltd., Beijing, China) at room temperature for 20 minutes, and then incubated with the rabbit anti-mouse

STAT3 monoclonal antibody (1:100, bsm-33223M, Beijing Bioss Biotechnology Co., Ltd., Beijing, China) overnight at 4°C. The sections were then incubated at 37°C for 30 minutes with the secondary antibody, biotinylated goat anti-rabbit immunoglobulin G (IgG; 1:1000, ab6789, Abcam, Inc., Cambridge, MA, USA). Streptomycin avidin-peroxidase solution was then added to the sections (Beijing Zhongshan Biotechnology Co., Ltd., Beijing, China), and reacted at 37°C for 20 minutes. The procedure regimens used were followed in accordance with a previous study.[18] Five high-power visual fields were randomly selected in each section, subsequently followed by measurement of the positive staining area, the rate of positive staining in the total area, and the average integral optical density (OD) or average intensity. Normal serum was used as negative control instead of the primary antibody, while the known positive sections were used as positive controls. RAD51AP1 was mainly stained at the nucleus. Second-level scoring was adopted for evaluation. First, the staining intensity was scored as 0, 1, 2, 3 or 4 points. The positive rate was then scored as: 0 point, no staining; 1 point, 1–25%; and 2 points, 26–50%. Finally, the sections were divided into low (< 8 points) and high (≥ 8 points) expression. A double-blind method was adopted to analyze the results, and professional pathologists independently read the sections.

Cell transfection

NSCLC cell lines A549 (human lung adenocarcinoma) and H520 (human lung squamous cell carcinoma) from the American Type Culture Collection (ATCC, Rockville, MD, USA) were subjected to culture in RPMI 1640 medium (HyClone, Logan, Utah, USA) containing 10% fetal bovine serum, 100 U/mL penicillin, and 100 U/mL streptomycin in an incubator (Thermo Fisher Scientific Inc., Waltham, MA, USA) at 37°C with 5% CO_2 and saturated humidity for 24 hours under sterile culture. A549 and H520 cells in the logarithmic growth phase were seeded into a six-well plate and transfected in strict accordance with the Lipofectamine 2000 (Invitrogen, Carlsbad, CA, USA) instructions when the cell density reached 30–50%. Cell transfection was conducted with negative control (NC) plasmid (universal negative control small interfering RNA [siRNA] purchased from Bioneer, Daejeon, Korea), RAD51AP1 vector (RAD51AP1 overexpression plasmid with the sequence of 5′-GGAATTGAAACCGCCGCTGAA-3′), or short hairpin (sh)-RAD51AP1 (shRNA targeting RAD51AP1 with the sequence of CCUCAUAUCUCUAAUUGCAUU). Cells without any transfection were regarded as a blank control. The aforementioned plasmids were purchased from Shanghai GenePharma Co. Ltd. (Shanghai, China). The

cells were subjected to culture with 5% CO_2 at 37°C for 6–8 hours, followed by another culture for 24–48 hours with complete medium, then by subsequent experiments.

RNA isolation and quantification

With the help of a Trizol extraction kit (RP2401, Beijing BioTeke Corporation, Beijing, China), the total RNA was extracted from the NSCLC tissues, adjacent normal lung tissues, human lung adenocarcinoma cell lines (A549, GLC82, SW1573, PG49), human lung squamous cell carcinoma (H520, MES-1, LTEP-s), and transfected A549 and H520 cells. The primer sequences (Table 2) were designed using Premier 5.0 software, and synthesized by Invitrogen Inc. Glyceraldehyde-3-phosphate dehydrogenase (GAPDH) was used as an internal reference. The extracted RNA was reverse transcribed into complementary DNA (cDNA) in strict accordance with the instructions of the Prime Script RT Kit (RR036A, Takara Biotechnology Co., Ltd. Dalian, China). The relevant primers were subjected to amplification and detection using the LightCycler 480 II real-time PCR instrument (480II, Roche Molecular Diagnostics Inc., South Branchburg, NJ, USA) according to the instructions of the SYBR Premix Ex TaqII kit (RR820A, Takara Biotechnology Co., Ltd.). Using 2 μg total RNA as a template,

Table 2 Primer sequences for RT-qPCR

Gene	Primer sequence
RAD51AP1	Forward: 5′-ATGACAAGCTCTACCAGAGAGAC-3′
	Reverse: 5′-CACATTAGTGGTGACTGTTGGAA-3′
E-cadherin	Forward: 5′-CGAGAGCTACACGTTCACGG-3′
	Reverse: 5′-GGGTGTCGAGGGGAAAAATAGG-3′
Occludin	Forward: 5′-ACAAGCGGTTTTATCCAGAGTC-3′
	Reverse: 5′-GTCATCCACAGGCGAAGTTAAT-3′
Cytokeratin	Forward: 5′-CAGCCAGCGTCTATGCAGG-3′
	Reverse: 5′-CTTTCTCGGTCTGGATTCCAC-3′
N-cadherin	Forward: 5′-TTTGATGGAGGTCTCCTAACACC-3′
	Reverse: 5′-ACGTTTAACACGTTGGAAATGTG-3′
Vimentin	Forward: 5′-GCCCTAGACGAACTGGGTC-3′
	Reverse: 5′-GGCTGCAACTGCCTAATGAG-3′
Fibronectin	Forward: 5′-TCTGTGCCTCCTATCTATGTGC-3′
	Reverse: 5′-GAGGGACCACGACAACTCTTC-3′
MMP-2	Forward: 5′-AGATCTTCTTCTTCAAGGACCGGTT-3′
	Reverse: 5′-GGCTGGTCAGTGGCTTGGGGTA-3′
OPN	Forward: 5′-CTGGTGCTCGTCCTCTACTAC-3′
	Reverse: 5′-GGACACGAAGGTAAAGGTGAC-3′
CD62	Forward: 5′-ACTGCCAGAATCGCTACACAG-3′
	Reverse: 5′-CACCCATGTCCATGTCTTATTGT-3′
TMP-2	Forward: 5′-ACGACTATGGTCGCGGATTC-3′
	Reverse: 5′-ACCGACAATCACGTCAGCTT-3′
GAPDH	Forward: 5′-AATGGGCAGCCGTTAGGAAA-3′
	Reverse: 5′-GCGCCCAATACGACCAAATC-3′

GAPDH, glyceraldehyde-3-phosphate dehydrogenase; RT-qPCR, reverse transcription quantitative PCR.

the transcription level of the target genes normalized to GAPDH was calculated on the basis of relative quantification ($2^{-\triangle\triangle Ct}$ method).

Western blot analysis

The total protein was extracted from human lung adenocarcinoma cell lines (A549, GLC82, SW1573, PG49), human lung squamous cell carcinoma (H520, MES-1, LTEP-s), and transfected A549 and H520 cells using a RIPA Kit (R0010, Beijing Solarbio Science & Technology Co. Ltd., Beijing, China). Subsequently, the protein was separated by performing polyacrylamide gel electrophoresis, and was then transferred onto a nitrocellulose membrane by wet transfer method. The membrane was then blocked using 5% bovine serum albumin at room temperature for one hour, and then incubated with the following diluted primary antibodies: rabbit polyclonal antibody to RAD51AP1 (1:1000, ab101321), E-cadherin (1:500, ab15148), occludin (1:1000, ab168986), CK (1:1000, ab9377), N-cadherin (1: 200, ab18203), vimentin (1:1000, ab137321), fibronectin (1:500, ab2413), MMP-2 (1:2000, ab37150), OPN (1:1000, ab8448), and CD62 (1:300, ab18981) (all from Abcam), and 2,4,4-trimethyl-2-pentene (TMP-2) (1:500, YJ70002149, Shanghai Yiji Industrial Co., Ltd., Shanghai, China) at 4°C overnight. The following day, the membrane was incubated with horseradish peroxidase-labeled rabbit anti-human IgG (1:5000, F020218, Beijing Biolab Science and Technology Co., Ltd., Beijing, China), followed by reaction with enhanced chemiluminescence solution (ECL808-25, Biomiga, San Diego, CA, USA), and then developed using a chemiluminescence detection system (ChemiDoc MP, Bio-Rad, Hercules, CA, USA). Using GAPDH (1:1000, ab8245, Abcam) as an internal reference, the relative expression of proteins was calculated as the ratio of gray values of target bands to that of internal reference.

Scratch test

After 48 hours of transfection, the A549 or H520 cell suspension was seeded into a six-well plate at a cell density of 1×10^5 cells/well. A sterile 200 μL tip head was used to horizontally and vertically draw four marks on the bottom of each well of equal strength. After removal of the original culture medium, 2 mL of serum-free solution was added to each well and incubated. The observations were photographed under an inverted microscope at 0 and 24 hours after scratching. Five visual fields in each sample were then randomly selected to count the cells. The width of multiple scratch points was measured. The scratch healing rate was calculated by: ([scratch width at 0 hour - scratch width at 24 hour]/scratch width at 0 hour × 100%).

Transwell assay

After 48 hours of transfection, the A549 and H520 cells in each group were resuspended with the cell density adjusted to 1×10^5 cells/mL. Subsequently, 200 μL of cell suspension was added to the apical chamber of the Transwell chamber paved with Matrigel gel (356234, Shanghai Shanran Biotechnology Co., Ltd., Shanghai, China) (1:8). A total of 600 μL of the RPMI 1640 medium containing 20% fetal bovine serum was added to the basolateral chamber. After routine incubation for 24 hours, the cells were fixed using 4% paraformaldehyde for 15 minutes and stained with 0.5% crystal violet solution prepared with methanol for 15 minutes. Five visual fields were then randomly selected and the cells were photographed under an inverted microscope (Axio Observer A1, Carl Zeiss AG, Oberkochen, Germany). The number of cells invading a chamber was counted. All investigations involved three duplicated wells, and each experiment was conducted in triplicate to obtain average values.

Hoechst 33342/propidium iodide double staining

The cell suspension was seeded into a 25 cm^2 cell culture flask at a density of $1–2 \times 10^4$ cells/mL, followed by the addition of 1 mL phosphate buffered saline (PBS) cell suspension + 10 μL Hoechst33342 (25 mg of Hoechst 33342 + 25 mL PBS was combined to prepare 10 μg/mL working concentration according to different volume requirements) (R0402, Shanghai Shifeng Biotechnology Co., Ltd., Shanghai, China). Cells were then incubated in a 37°C incubator for 15 minutes, after which 30 μL of PBS cell suspension +10 μL 50 μmol/L propidium iodide (PI) was added (5 mg PI + l rnL PBS was used to prepare 5×10^3 g/mL PI stock solution, followed by preparation of 50 μg/mL working concentration according to different volume requirements) (R0402, Shanghai Shifeng Biotechnology Co., Ltd.). The morphological characteristics of the nucleus were observed under a fluorescence microscope (Axio Observer A1, Carl Zeiss AG) at an excitation wavelength of 380 nm and an absorption wavelength of 420 nm.

Cell-counting kit 8

After transfection for 24 hours, the cells were prepared into a single cell suspension. After counting, the single cell suspension was seeded into a 96-well plate at a density of $3 \times 10^3–6 \times 10^3$ cells/well (200 μL per well), and then cultured in an incubator with six duplicated wells set. The cells were cultured for 24, 48, or 72 hours, separately. Next, 10 μL Cell Counting Kit 8 (CCK-8) reagent (Sigma-

Aldrich, San Francisco, CA, USA) was added into each well for another two hour culture procedure. The OD values at 450 nm were measured using an enzyme-linked immunosorbent assay reader (ELx800, BioTek, Winooski, VT, USA). The cell viability curve was drawn with the time points as the abscissa and the OD values as the ordinate.

Cell colony formation assay

The A549 and H520 cell lines were prepared into a cell suspension and counted. The A549 and H520 cell lines in each group were seeded into a six-well plate (9.6 cm^2) at a density of 500 cells/well. Subsequently, 4 mL of cell culture medium was added to the cell lines at 37°C, and cultured in a 37°C incubator. The culture was terminated upon observation of the colony. Cells were fixed using 5 mL of 4% paraformaldehyde for 15 minutes and then stained with GIMSA dye solution for 10–30 minutes. The cell clone formation rate was calculated by: (the number of cloned cells/the number of seeded cells) × 100%.

Xenograft tumor in nude mice

The A549 and H520 cell lines (Clone 9) consistently expressing luciferase were prepared into a single cell suspension and resuspended in a mixture of PBS and Matrigel (1:1) to attain the final concentration of 1×10^6 cells/200 μL. Nude mice were provided by the Experimental Pathology Laboratory of Shanghai Cancer Research Institute for experiments (production license number: SCXK Shanghai 2002–0001; approval license number SYXK Shanghai 2002–0009). After anesthetizing with diethyl ether, the nude mice were subcutaneously seeded with the transfected A549 and H520 cells (1×10^6 cells/200 μL) via the axilla. The mice were then kept in the same environment and observed every seven days. The length and width of the tumor were documented, and the tumor volume was calculated on the basis of the formula: volume = length × width^2/2. After 28 days, the nude mice were euthanized and the tumors were collected by dissection. RAD51AP1 expression in the tumor tissues of nude mice was detected by performing reverse transcription quantitative PCR (RT-qPCR).

Statistical analysis

Statistical analysis was performed using SPSS version 19.0. Count data were presented as percentages and the measurement data were expressed as mean ± standard deviation. Comparison of the count data between two groups was performed by chi-square test, and the comparison of measurement data was performed by *t* test. Comparison of measurement data among multiple groups was assessed by one-way analysis of variance (ANOVA) and data at different time points were analyzed by repeated measures ANOVA. $P < 0.05$ indicated that the differences were statistically significant.

Results

Highly expressed RAD51AP1 is found in non-small cell lung cancer (NSCLC)

Initially, DEGs were screened from microarray data of NSCLC in the GEO database. According to the screening threshold of |log2FC| > 2.0 and adj.p.al < 0.05, 634, 961, 959, and 2177 DEGs were screened from the GSE19188, GSE101929, GSE33532, and GSE74706 datasets, respectively. The top 400 genes of each dataset were then compared, after which a Venn diagram was drawn (Fig 1a), which revealed the presence of 74 intersected genes. The PPI network of the NSCLC-associated DEGs was constructed on the basis of existing information of gene interaction provided by the String database. As shown in Figure 1b, the DEGs associated with other genes in this network were *AURKA*, *UBE2C*, *CEP55*, *KIAA0101*, *ZWINT*, *DLGAP5*, *MELK*, *RAD51AP1*, and *UBE2T* (degree > 5). We speculated that these nine genes might play an important role in NSCLC. In order to further explore the relationship between DEGs and NSCLC, Chilibot was employed to construct the relationship network between these nine DEGs and NSCLC (Fig 1c). The remaining eight genes, except *RAD51AP1*, were observed to be directly or indirectly associated with NSCLC, suggesting that *RAD51AP1* has been poorly studied in NSCLC. The heat maps of the top 100 DEGs in GSE19188 and GSE101929 datasets are shown in Figure 1d,e, respectively, suggesting that the *RAD51AP1* gene was highly expressed in NSCLC. The GSE33532 and GSE74706 microarray datasets (Fig 1f,g) showed higher expression of RAD51AP1 in NSCLC tumor tissues than that in adjacent normal lung tissues. Therefore, RAD51AP1 was selected for subsequent experiments.

Positive expression rate of RAD51AP1 protein is elevated in NSCLC tissues

To further evaluate the expression of RAD51AP1 in NSCLC, immunohistochemistry (IHC) was adopted to measure the positive expression rate of the RAD51AP1 protein among the 91 cases of NSCLC tissues and adjacent normal lung tissues. As depicted in Figure 2, RAD51AP1 protein expression was observed in both the NSCLC tissues and adjacent normal lung tissues. Positive cells were reflected by the presence of yellow particles in the nucleus. Among the NSCLC tissue samples (*n* = 91), 57 cases (63%)
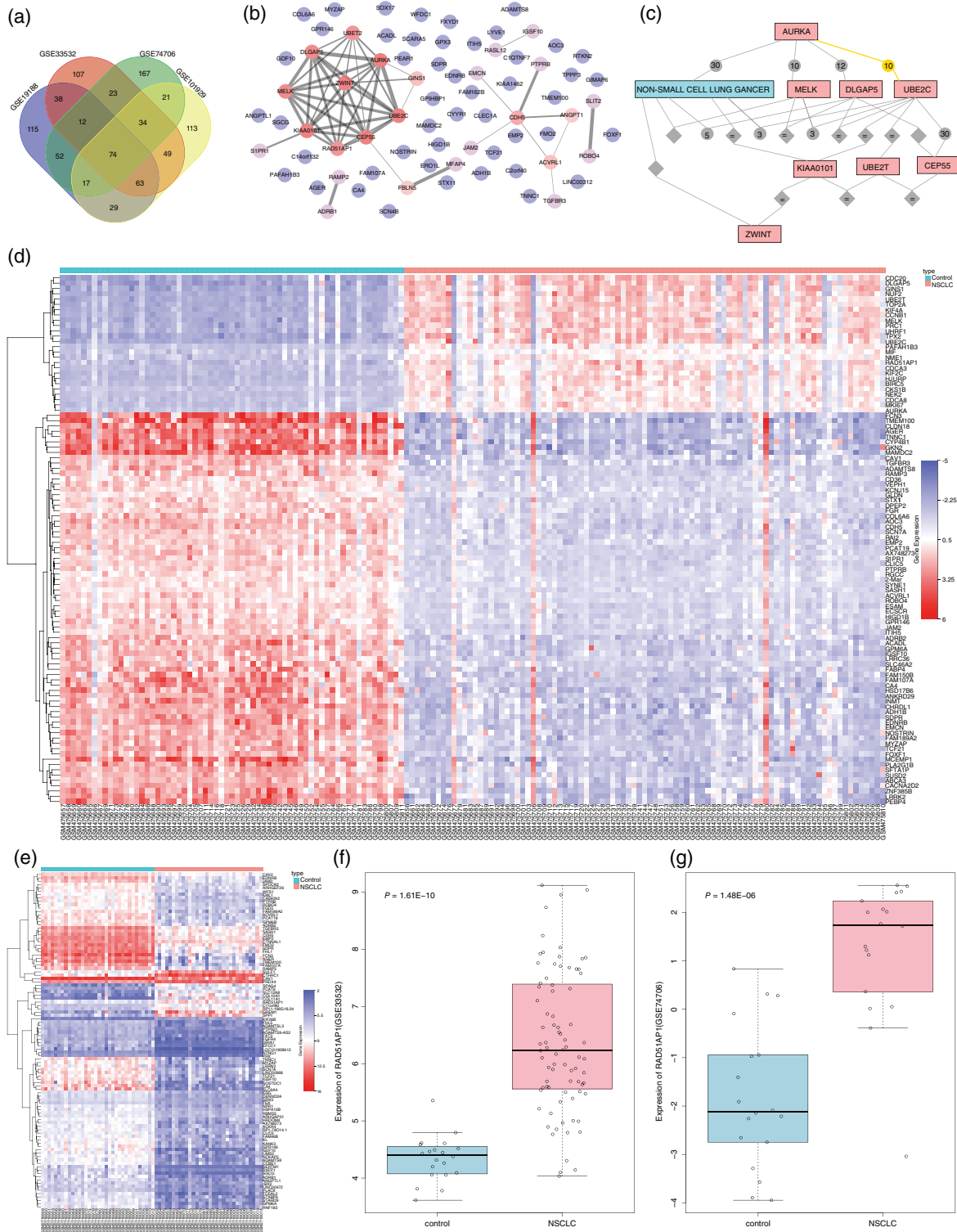
Figure 1 RAD51AP1 is predicted to be involved in non-small cell lung cancer (NSCLC). (**a**) The intersection of differentially expressed genes (DEGs) screened from GSE19188, GSE101929, GSE33532, and GSE74706 datasets, suggesting 74 intersected genes. (**b**) The interaction network of NSCLC-related DEGs. (**c**) The relationship network between NSCLC-related DEGs and NSCLC. (**d,e**) The heat maps of the top 100 DEGs in GSE19188 and GSE101929 datasets, respectively. The abscissa represents the sample number, and the ordinate represents the DEGs. The histogram at the upper right refers to the color gradation, and each rectangle corresponds to a sample expression value. (**f,g**) RAD51AP1 expression in GSE33532 and GSE74706 datasets, respectively.

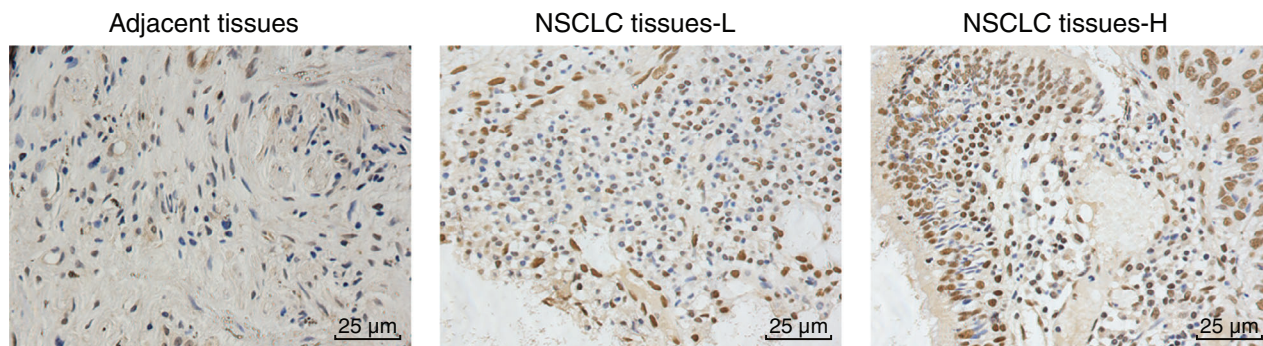| Adjacent tissues	NSCLC tissues-L	NSCLC tissues-H

Figure 2 The positive expression rate of RAD51AP1 protein is increased in non-small cell lung cancer (NSCLC) tissues. RAD51AP1 protein in adjacent normal lung tissues was stained as weakly positive by immunohistochemistry (IHC) (×400; Normal: IHC score: 1), RAD51AP1 protein in NSCLC tissues was stained as weakly positive (×400; Tumor-Low: IHC score: 2) and strong positive (×400; Tumor-High: IHC score: 12) by IHC.

showed a high positive expression rate of RAD51AP1 protein (≥ 8 points), while 34 cases (37%) among the adjacent normal lung tissues ($n = 91$) exhibited a high positive expression rate of RAD51AP1 protein. These findings demonstrate that the proportion of positive RAD51AP1 protein expression in NSCLC tissues was significantly higher than in adjacent normal lung tissues ($P < 0.05$).

Subsequently, the clinical data of the 91 NSCLC patients enrolled in the study were analyzed, with further evaluation of the relationship between the clinical parameters of these patients and the expression of RAD51AP1 protein. No direct correlation was observed among the expression of RAD51AP1 and parameters such as patient age, gender, pathological types, and other parameters ($P > 0.05$). Compared to patients at stage I–II, the positive expression rate of RAD51AP1 protein was markedly enhanced in patients at stage III. The positive expression rate of RAD51AP1 protein in the tissues of patients with low differentiation was significantly higher than that observed in the tissues of patients with moderate and high differentiation (Table 3). Conjointly, these data support the conclusion that RAD51AP1 is expressed at a high level in NSCLC.

RAD51AP1 is expressed at a high level, and epithelial–mesenchymal transition (EMT) is induced in NSCLC

The aforementioned findings revealed an increased expression rate of the RAD51AP1 protein in NSCLC, with subsequent detection of messenger RNA (mRNA) and protein expression of RAD51AP1, EMT, and metastasis-related genes in NSCLC. As illustrated in Figure 3, compared to adjacent normal lung tissues, the mRNA and protein expression of RAD51AP1, N-cadherin, vimentin, fibronectin (interstitial cell marker protein), MMP-2, OPN, CD62, and TMP-2 (factors promoting tumor cell metastasis) was higher ($P < 0.05$),

Table 3 Relationship between RAD51AP1 expression and clinicopathological parameters of patients with NSCLC (*n*, %)

Clinical features	RAD51AP1		*P*
	Low expression	High expression	
Gender			0.392
Male	19 (33.93%)	37 (66.07%)	
Female	15 (42.86%)	20 (57.14%)	
Age (median age = 58 years)			0.698
< 58	10 (34.48%)	19 (65.52%)	
≥ 58	24 (38.71%)	38 (61.29%)	
Smoking			0.89
Non-smoker	5 (35.71%)	9 (64.29%)	
Smoker	29 (37.66%)	48 (62.34%)	
Combined cardiopulmonary chronic diseases			0.566
Yes	20 (40.00%)	30 (60.00%)	
No	14 (34.15%)	27 (65.85%)	
Clinical stage			0.041
I–II	23 (46.94%)	26 (53.06%)	
III	11 (26.19%)	31 (73.81%)	
Metastasis (pN)			0.334
N0–N1	22 (41.51%)	31 (58.49%)	
N2	12 (31.58%)	26 (68.42%)	
Pathological type			0.391
Squamous cell carcinoma	21 (42.86%)	28 (57.14%)	
Adenocarcinoma	10 (28.57%)	25 (71.43%)	
Other	3 (42.86%)	4 (57.14%)	
Organizational rating			0.016
Moderate and high differentiation	29 (45.31%)	35 (54.69%)	
Low differentiation	5 (18.52%)	22 (81.48%)	

NSCLC, non-small cell lung cancer.

while that of E-cadherin, occludin, and CK was lower ($P < 0.05$) in NSCLC tissues. From these findings, it can be concluded that RAD51AP1 is highly expressed, which facilitates EMT in NSCLC.

Figure 3 RAD51AP1 upregulation and induction of epithelial–mesenchymal transition (EMT) are detected in non-small cell lung cancer (NSCLC) tissues. (**a**) Messenger RNA (mRNA) and (**b,c**) protein expression of RAD51AP1, E-cadherin, occludin, cytokeratin, N-cadherin, vimentin, fibronectin, MMP-2, OPN, CD62, and TMP-2 in NSCLC tissues, with the protein bands assessed. *$P < 0.05$ versus adjacent normal lung tissues. GAPDH, glyceraldehyde-3-phosphate dehydrogenase.
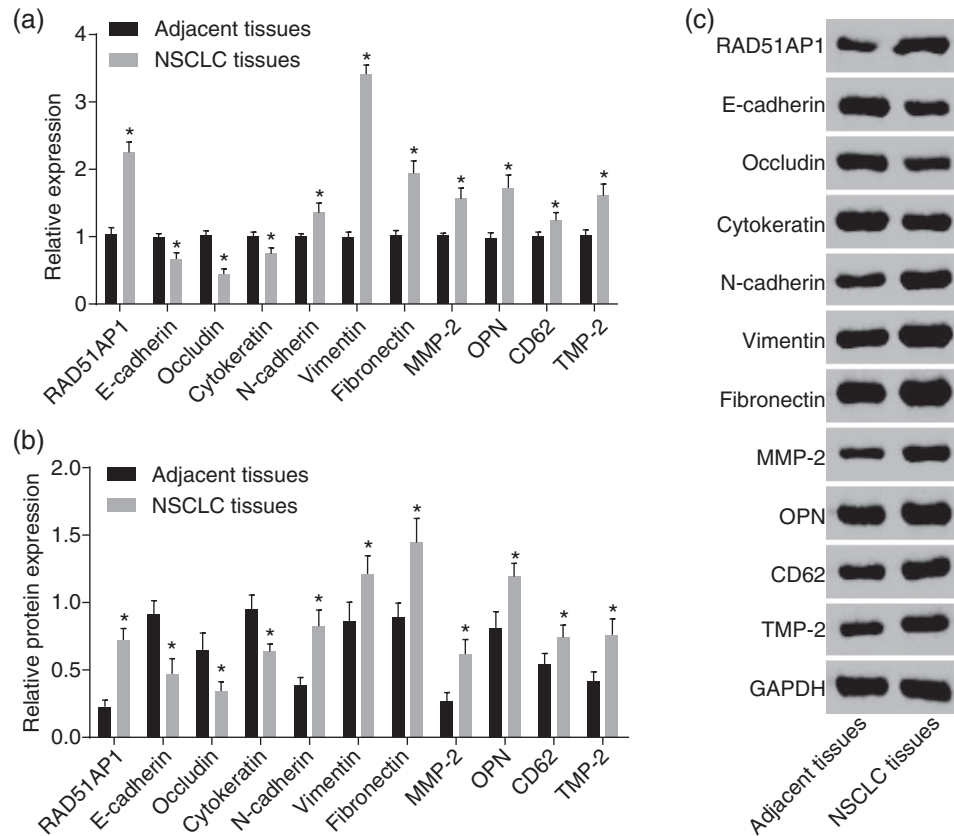
RAD51AP1 is highly expressed in A549 and H520 cell lines

RT-qPCR and Western blot analysis were conducted to detect the mRNA and protein expression of RAD51AP1 in lung adenocarcinoma (A549, GLC82, SW1573, and PG49) and lung squamous cell carcinoma (H520, MES-1, and LTEP-s) cell lines. As shown in Figure 4, the mRNA and protein expression of RAD51AP1 was significantly higher in the A549 and H520 cell lines compared to the other cell lines. Therefore, the A549 and H520 cell lines were selected for subsequent experiments.

RAD51AP1 silencing suppresses EMT in NSCLC cells

Previous results presented with upregulated RAD51AP1 and promoted EMT in NSCLC tissues, which initiated an investigation of the function of RAD51AP1 gene-mediating
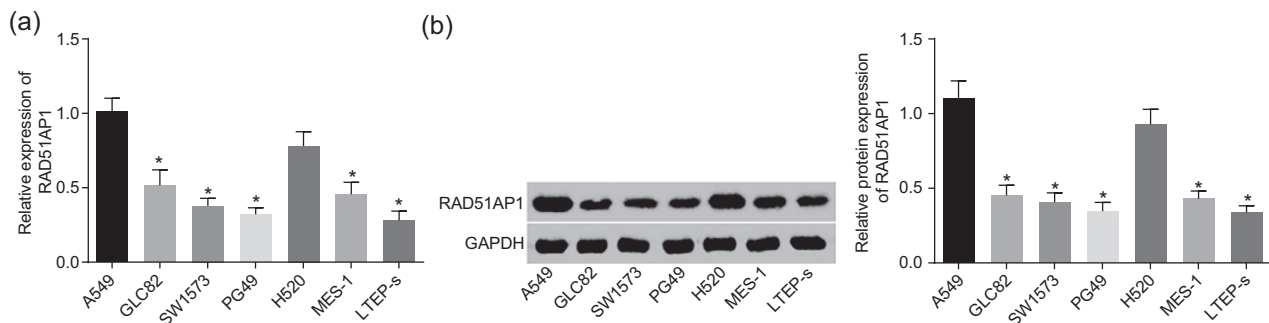

Figure 4 A549 and H520 cell lines exhibit the highest RAD51AP1 expression. (**a**) Messenger RNA (mRNA) expression of RAD51AP1 in cell lines A549, GLC82, SW1573, PG49, H520, MES-1, and LTEP-s detected by reverse transcription-quantitative PCR (RT-qPCR). (**b**) Protein expression of RAD51AP1 in cell lines A549, GLC82, SW1573, PG49, H520, MES-1, and LTEP-s examined by Western blot analysis. Statistics showed that the highest RAD51AP1 expression emerged in A549 and H520 cell lines. *$P < 0.05$ versus A549 or H520 cell lines.
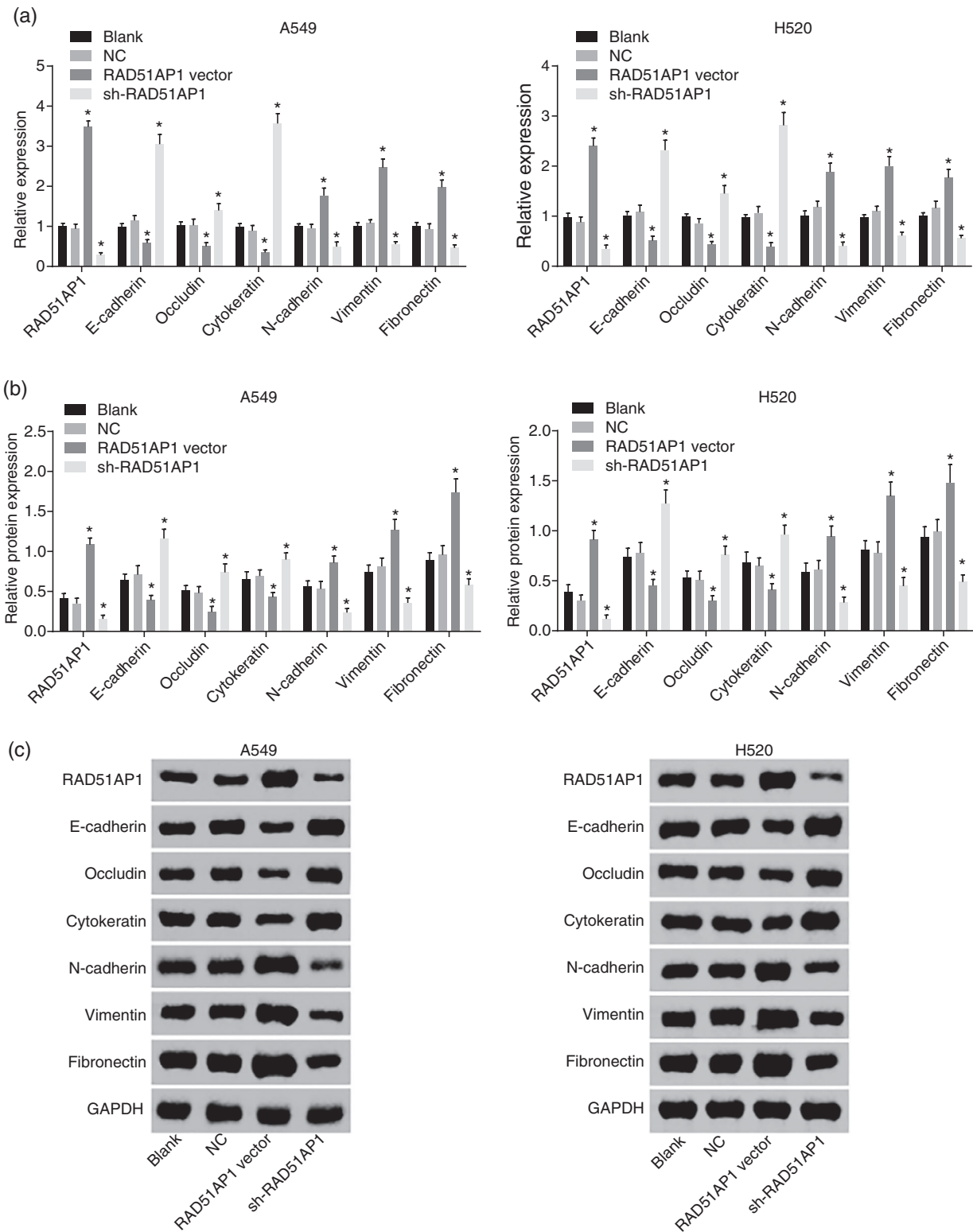
Figure 5 RAD51AP1 silencing reverses the induction of epithelial–mesenchymal transition (EMT) in non-small cell lung cancer (NSCLC) cells. (**a**) Messenger RNA (mRNA) and (**b,c**) protein expression of E-cadherin, occludin, cytokeratin, N-cadherin, vimentin, and fibronectin in A549 and H520 cell lines transfected with overexpressed or downregulated RAD51AP1, with protein bands assessed. *$P < 0.05$ versus the blank control and the negative control (NC) (cells without transfection or transfected with NC). GAPDH, glyceraldehyde-3-phosphate dehydrogenase; shRAD51AP1, small hairpin RAD51AP1.
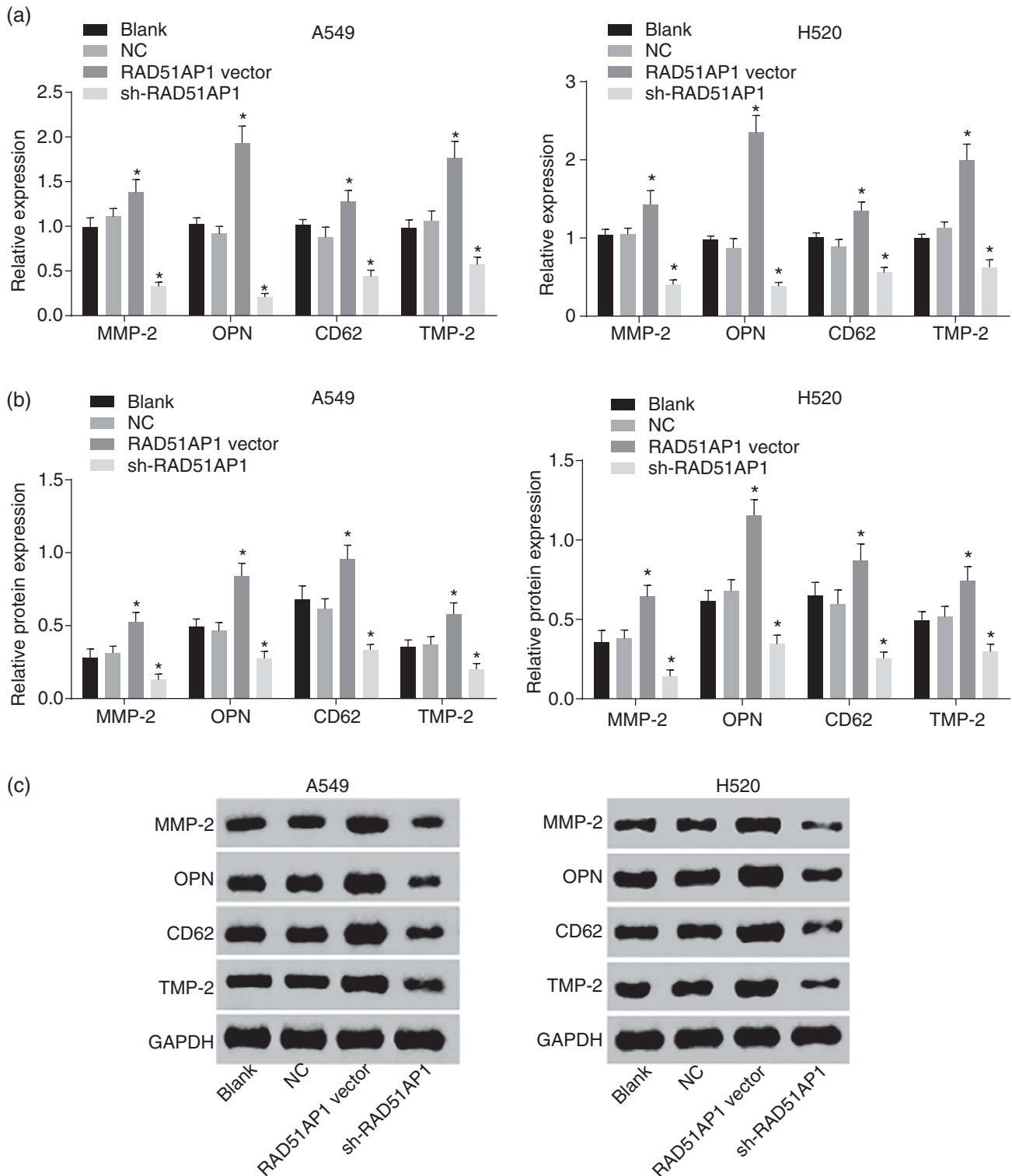
Figure 6 RAD51AP1 silencing exerts suppressive effects on the metastasis of non-small cell lung cancer (NSCLC) cells. (**a**) Messenger RNA (mRNA) and (**b,c**) protein expression of MMP-2, OPN, CD62, and TMP-2 in A549 and H520 cell lines transfected with overexpressed or silenced RAD51AP1, with protein bands assessed. *$P < 0.05$ versus the blank control and the negative control (NC) (cells without transfection or transfected with NC). GAPDH, glyceraldehyde-3-phosphate dehydrogenase; shRAD51AP1, small hairpin RAD51AP1.
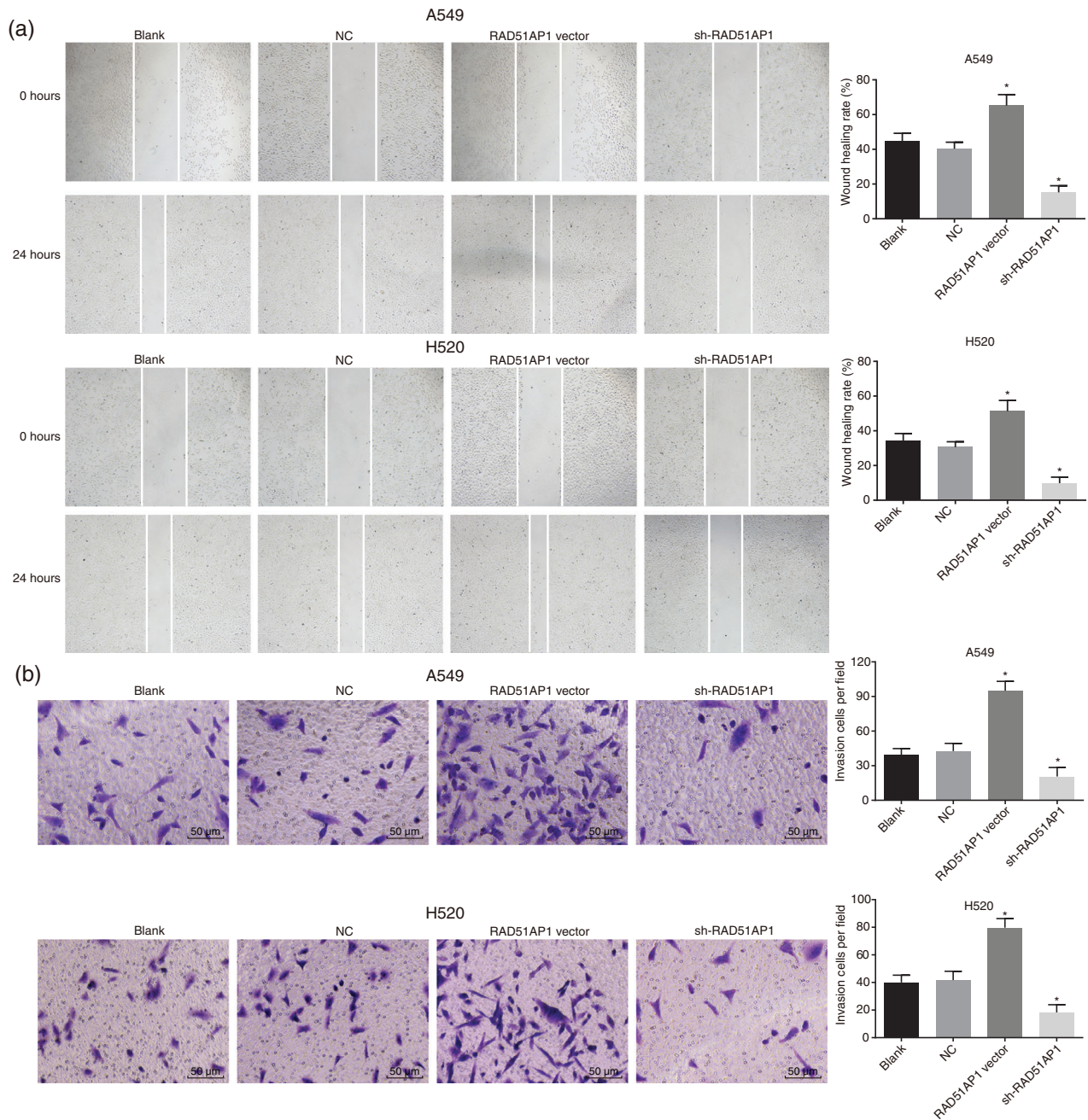
Figure 7 RAD51AP1 silencing inhibits non-small cell lung cancer (NSCLC) cell migration and invasion. Effects of RAD51AP1 on migration of A549 and H520 cell lines (**a**) by scratch test (×40) and (**b**) by Transwell assay (×200). *$P < 0.05$ versus the blank control and the negative control (NC) (cells without transfection or transfected with NC). shRAD51AP1, small hairpin RAD51AP1.

EMT in NSCLC cells. RT-qPCR and Western blot analysis results showed that the mRNA and protein expression of RAD51AP1, N-cadherin, vimentin, and fibronectin was increased ($P < 0.05$), while that of E-cadherin, occludin, and CK was decreased in A549 and H520 cell lines upon overexpression of RAD51AP1 ($P < 0.05$); these changes were contradictory in A549 and H520 cell lines after RAD51AP1 silencing mediated by sh-RAD51AP1

($P < 0.05$) (Fig 5). These results demonstrate that downregulation of RAD51AP1 represses EMT in NSCLC cells.

RAD51AP1 silencing prevents the metastasis of NSCLC cells

Subsequently, the effects of RAD51AP1 on NSCLC metastasis were investigated. The results of RT-qPCR and

Western blot analysis exhibited elevated mRNA and protein expression of MMP-2, OPN, CD62, and TMP-2 in A549 and H520 cell lines in response to RAD51AP1 over-expression ($P < 0.05$), whereas reduced expression was observed in A549 and H520 cell lines after sh-RAD51AP1 transfection ($P < 0.05$) (Fig 6). Thus, RAD51AP1 silencing suppresses the metastasis of NSCLC cells.

RAD51AP1 silencing inhibits cell migration, invasion, and proliferation yet induces apoptosis in NSCLC

Considering the regulation of RAD51AP1 in EMT markers and metastasis-related genes, the study focal point shifted to the potential effects of RAD51AP1 on A549 and H520 cellular behavior with RAD51AP1 overexpressed or silenced in A549 and H520 cells. The results of scratch testing and Transwell assay revealed stimulated cell migration and invasion after RAD51AP1 overexpression ($P < 0.05$), but repressed cell migration and invasion after sh-RAD51AP1 treatment ($P < 0.05$) (Fig 7). As shown in Figure 8, the number of apoptotic and necrotic cells significantly reduced after RAD51AP1 overexpression ($P < 0.01$), whereas the numbers increased after sh-RAD51AP1 treatment ($P < 0.01$). The viability of cells was observed at 24, 48, and 72 hours. CCK-8 results exhibited no significant difference in cell viability among the groups at zero hours ($P > 0.05$) (Fig 9a). In comparison to the viability of cells at zero hours, significant increases were evident in cell viability at 24, 48 and 72 hours (all $P < 0.05$). The

cell viability was remarkably elevated after RAD51AP1 overexpression ($P < 0.05$), while it was reduced after sh-RAD51AP1 treatment ($P < 0.05$). The results of cell colony formation assay (Fig 9b,c) illustrated an enhanced clone formation rate after RAD51AP1 overexpression ($P < 0.05$), and a decreased formation rate after sh-RAD51AP1 treatment ($P < 0.05$). The changes in the behavior of A549 cells were all consistent with those in H520 cells. These results support the conclusion that downregulation of RAD51AP1 has an inhibitory effect on the proliferation, migration, and invasion of NSCLC cells and a simulative effect on cell apoptosis.

RAD51AP1 silencing inhibits tumor growth in vivo

Finally, xenograft tumors in nude mice were applied to determine the effects of RAD51AP1 on tumor growth. The results showed increased tumor weight and volume in nude mice after RAD51AP1 overexpression ($P < 0.05$), while a reduction was observed after RAD51AP1 silencing ($P < 0.05$) (Fig 10). The results suggest that silencing of RAD51AP1 could reduce tumor formation and growth in vivo.

Discussion

NSCLC represents one of the major causes of cancer-associated mortality around the world.[19] Failure to treat advanced NSCLC has been ascribed to distant metastasis,
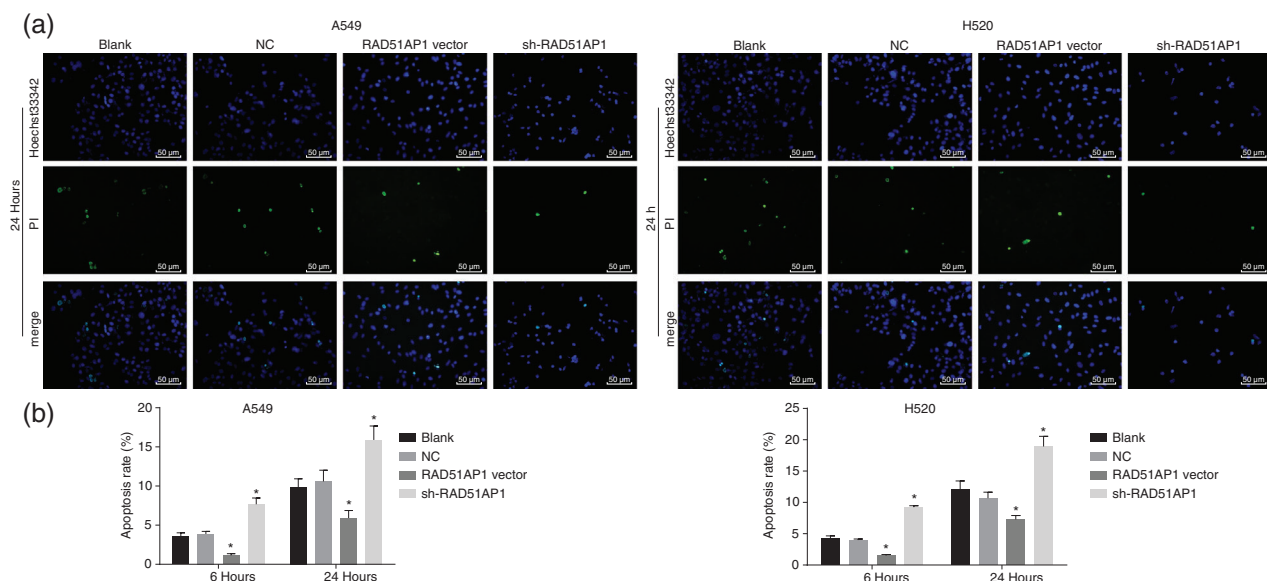

Figure 8 RAD51AP1 silencing exerts suppressive effects on non-small cell lung cancer (NSCLC) cell apoptosis. (**a**) The apoptosis and necrosis of A549 and H520 cell lines under fluorescence microscope (200×). (**b**) The apoptosis and necrosis rates of A549 and H520 cell lines transfected with over-expressed or silenced RAD51AP1. *$P < 0.05$ versus the blank control and the negative control (NC) (cells without transfection or transfected with NC).
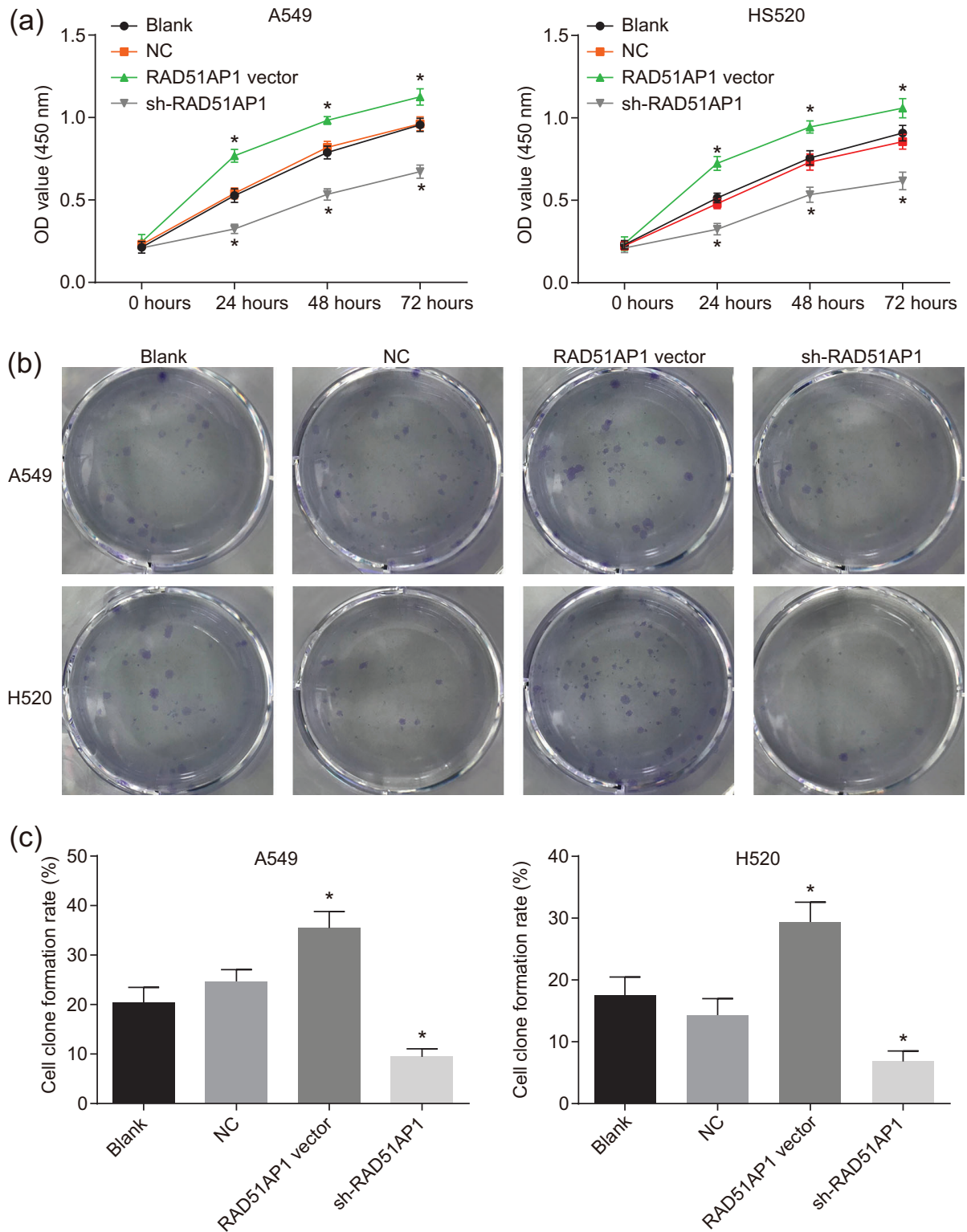
Figure 9 Silencing of RAD51AP1 represses non-small cell lung cancer (NSCLC) cell proliferation and clone formation ability. (**a**) The proliferation of A549 and H520 cell lines at 0, 24, 36, and 48 hours in response to RAD51AP1 overexpression or silencing detected by Cell Counting Kit 8 (CCK-8) assay. (**b**) Colony formation ability and (**c**) clone formation rate of A549 and H520 cell lines in response to RAD51AP1 overexpression or silencing. *$P < 0.05$ versus the blank control and the negative control (NC) (cells without transfection or transfected with NC). shRAD51AP1, small hairpin RAD51AP1.
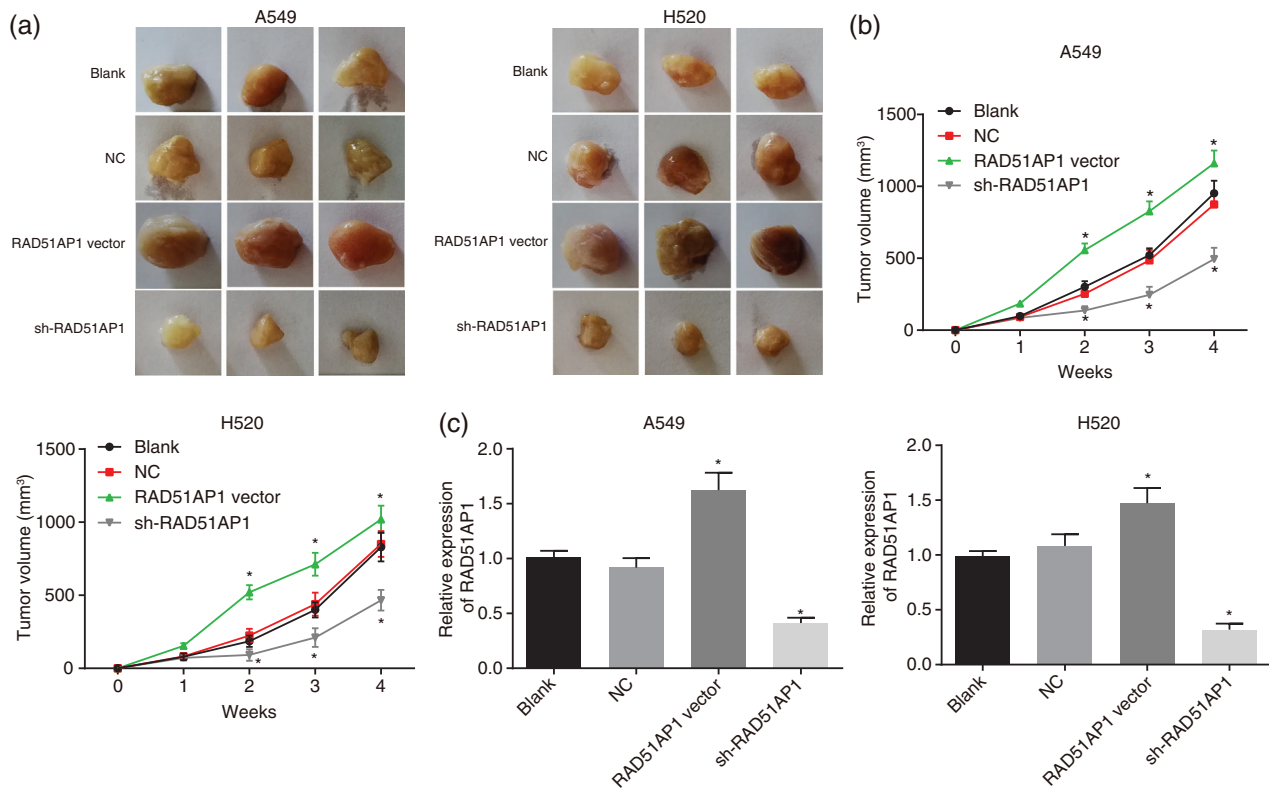
Figure 10 Silencing of RAD51AP1 inhibits tumor growth in vivo. (**a**) Representative images of tumors after dissection from nude mice in response to RAD51AP1 overexpression or silencing after 28 days. (**b**) Tumor growth curve of nude mice in response to RAD51AP1 overexpression or silencing. (**c**) The expression of RAD51AP1 in tumor tissues of nude mice in response to RAD51AP1 overexpression or silencing detected by reverse transcription quantitative PCR (RT-qPCR). *$P < 0.05$ versus the blank control and the negative control (NC) (nude mice injected with untransfected or NC-transfected cells). shRAD51AP1, small hairpin RAD51AP1.

which is strongly associated with prognosis in NSCLC.[20] Epithelial cell markers (such as E-cadherin) are lost and typical mesenchymal markers appear in the process of EMT, which is associated with poor survival in NSCLC.[21] Thus, our study aimed to investigate the potential role of the *RAD51AP1* gene in the EMT and metastasis of NSCLC. Collectively, the findings from this study demonstrate that downregulated RAD51AP1 prevents the development of NSCLC by attenuating EMT and metastasis in NSCLC cells.

The initial finding of this study revealed high expression of RAD51AP1 in NSCLC tissues. Previous research has reported elevated RAD51AP1 expression in lung cancer.[9] Furthermore, recent evidence has demonstrated the correlation of high RAD51AP1 expression with poor survival in lung adenocarcinoma.[10] *RAD51B* overexpression has been observed in male NSCLC patients with squamous cell carcinoma, *EGFR* mutation, and no *KRAS* mutation.[22] Our findings are consistent with these results, speculating the involvement of RAD51AP1 in NSCLC. Additionally, our findings demonstrate that downregulation of RAD51AP1 could reduce EMT of NSCLC as a result of the lower

expression of various mesenchymal markers (N-cadherin, vimentin, fibronectin) and elevated expression of various epithelial markers (E-cadherin, occludin, CK). A previous report clarified and documented the observation of a loss of E-cadherin and gain of vimentin and fibronectin during EMT.[23] Vimentin and E-cadherin play key roles in EMT, for instance, downregulation of E-cadherin subsequently leads to deprived epithelial morphology and an acquired aggressive mesenchymal phenotype.[24] Existing literature supports the involvement of upregulated vimentin in cell migration and tissue invasion, as well as poor survival in resected NSCLC patients.[25] Evidence has been presented of the regulation of various epithelial markers (E-cadherin, occludin, and CK18) and mesenchymal markers (such as N-cadherin) by MUC4, which promotes invasion and metastasis in pancreatic cancer.[26] Moreover, a reduction in the expression of SIM2s leads to deprived homologous recombination efficiency by disrupting RAD51 recruitment, thus ultimately resulting in genomic instability and EMT induction.[27] Downregulated AXL has been documented to repress RAD51 (a protein closely related to homologous recombination) and EMT in NSCLC.[28]

Collectively, the obtained evidence supports the theory that RAD51AP1 silencing inhibits EMT of NSCLC.

Another significant finding of our study showed that RAD51AP1 silencing treatment resulted in a significant decline in NSCLC cell metastasis, which was indicated upon observation of the decreased expression of metastasis-related factors (MMP-2, OPN, CD62, and TMP-2) after the knockdown of RAD51AP1. The association between OPN (a secret phosphorylated glycoprotein) and MMPs has been highlighted with tumor metastasis in NSCLC.[29] Downregulation of CDDC6 facilitates low expression of RAD51 and is strongly related to the production of lymph node metastasis in NSCLC.[30] Additionally, our findings demonstrate that downregulation of RAD51AP1 can reduce proliferation, invasion, and migration, but also stimulates the apoptosis of NSCLC cells. RAD51 has been documented to be of key importance in poor survival of NSCLC patients and inhibition of NSCLC cell apoptosis.[31] RAD51 is also highly expressed in NSCLC and could suppress tumor cell apoptosis.[32] On the basis of the aforementioned evidence, it can be concluded that RAD51AP1 silencing can reduce metastasis, proliferation, invasion, and migration, but induce apoptosis of NSCLC cells.

In conclusion, evidence obtained from this study shows that downregulation of RAD51AP1 can potentially suppress the metastasis and EMT of NSCLC cells. These results suggest that further understanding of the molecular mechanism underlying NSCLC may have promising clinical implications for treatment. However, further study with a larger sample is warranted in order to acquire comparatively higher accuracy of results. Additionally, a more comprehensive study should be conducted in order to obtain more details related to the mechanism of EMT and metastasis in NSCLC.

Acknowledgment

Disclosure

No authors report any conflict of interest.

References

1 Torre LA, Siegel RL, Jemal A. Lung cancer statistics. *Adv Exp Med Biol* 2016; **893**: 1–19.

2 Ettinger DS, Wood DE, Akerley W *et al.* Non-small cell lung cancer, version 1.2015. *J Natl Compr Canc Netw* 2014; **12**: 1738–61.

3 Fan H, Shao ZY, Xiao YY *et al.* Incidence and survival of non-small cell lung cancer in Shanghai: A population-based cohort study. *BMJ Open* 2015; **5**: e009419.

4 Stemmler MP, Eccles RL, Brabletz S, Brabletz T. Non-redundant functions of EMT transcription factors. *Nat Cell Biol* 2019; **21**: 102–12.

5 Huang R, Zong X. Aberrant cancer metabolism in epithelial-mesenchymal transition and cancer metastasis: Mechanisms in cancer progression. *Crit Rev Oncol Hematol* 2017; **115**: 13–22.

6 Chu SC, Hsieh YS, Hsu LS, Chen KS, Chiang CC, Chen PN. *Rubus idaeus* L inhibits invasion potential of human A549 lung cancer cells by suppression epithelial-to-mesenchymal transition and Akt pathway in vitro and reduces tumor growth in vivo. *Integr Cancer Ther* 2014; **13**: 259–73.

7 Zhong X, Luo G, Zhou X *et al.* Rad51 in regulating the radiosensitivity of non-small cell lung cancer with different epidermal growth factor receptor mutation status. *Thorac Cancer* 2016; **7**: 50–60.

8 Pires E, Sung P, Wiese C. Role of RAD51AP1 in homologous recombination DNA repair and carcinogenesis. *DNA Repair (Amst)* 2017; **59**: 76–81.

9 Chudasama D, Bo V, Hall M *et al.* Identification of cancer biomarkers of prognostic value using specific gene regulatory networks (GRN): A novel role of RAD51AP1 for ovarian and lung cancers. *Carcinogenesis* 2018; **39**: 407–17.

10 Li S, Xuan Y, Gao B *et al.* Identification of an eight-gene prognostic signature for lung adenocarcinoma. *Cancer Manag Res* 2018; **10**: 3383–92.

11 Nguyen TTT, Park EM, Lim YS, Hwang SB. Nonstructural protein 5A impairs DNA damage repair: Implications for hepatitis C virus-mediated hepatocarcinogenesis. *J Virol* 2018; **92**: pii: e00178–18.

12 Obama K, Satoh S, Hamamoto R, Sakai Y, Nakamura Y, Furukawa Y. Enhanced expression of RAD51 associating protein-1 is involved in the growth of intrahepatic cholangiocarcinoma cells. *Clin Cancer Res* 2008; **14**: 1333–9.

13 Gautier L, Cope L, Bolstad BM, Irizarry RA. affy--analysis of Affymetrix GeneChip data at the probe level. *Bioinformatics* 2004; **20**: 307–15.

14 Smyth GK. Linear models and empirical bayes methods for assessing differential expression in microarray experiments. *Stat Appl Genet Mol Biol* 2004; **3**: Article3.

15 Szklarczyk D, Franceschini A, Wyder S *et al.* STRING v10: Protein-protein interaction networks, integrated over the tree of life. *Nucleic Acids Res* 2015; **43**: D447–52.

16 Shannon P, Markiel A, Ozier O *et al.* Cytoscape: A software environment for integrated models of biomolecular interaction networks. *Genome Res* 2003; **13**: 2498–504.

17 Chen H, Sharp BM. Content-rich biological network constructed by mining PubMed abstracts. *BMC Bioinf* 2004; **5**: 147.

18 Alshareeda AT, Negm OH, Aleskandarany MA et al. Clinical and biological significance of RAD51 expression in breast cancer: A key DNA damage response protein. Breast Cancer Res Treat 2016; **159**: 41–53.

19 Reck M, Heigener DF, Mok T, Soria JC, Rabe KF. Management of non-small-cell lung cancer: Recent developments. Lancet 2013; **382**: 709–19.

20 Wang R, Chen XF, Shu YQ. Prediction of non-small cell lung cancer metastasis-associated microRNAs using bioinformatics. Am J Cancer Res 2015; **5**: 32–51.

21 Chen Y, Lu L, Feng B et al. Non-coding RNAs as emerging regulators of epithelial to mesenchymal transition in non-small cell lung cancer. Oncotarget 2017; **8**: 36787–99.

22 Wu M, Sheng Z, Jiang L, Liu Z, Bi Y, Shen Y. Overexpression of RAD51B predicts a preferable prognosis for non-small cell lung cancer patients. Oncotarget 2017; **8**: 91471–80.

23 Xu G, Yu H, Shi X et al. Cisplatin sensitivity is enhanced in non-small cell lung cancer cells by regulating epithelial-mesenchymal transition through inhibition of eukaryotic translation initiation factor 5A2. BMC Pulm Med 2014; **14**: 174.

24 Luo W, Fang W, Li S, Yao K. Aberrant expression of nuclear vimentin and related epithelial-mesenchymal transition markers in nasopharyngeal carcinoma. Int J Cancer 2012; **131**: 1863–73.

25 Saito N, Mine N, Kufe DW, von Hoff D, Kawabe T. CBP501 inhibits EGF-dependent cell migration, invasion and epithelial-to-mesenchymal transition of non-small cell lung

cancer cells by blocking KRas to calmodulin binding. Oncotarget 2017; **8**: 74006–18.

26 Rachagani S, Macha MA, Ponnusamy MP et al. MUC4 potentiates invasion and metastasis of pancreatic cancer cells through stabilization of fibroblast growth factor receptor 1. Carcinogenesis 2012; **33**: 1953–64.

27 Pearson SJ, Roy Sarkar T, McQueen CM et al. ATM-dependent activation of SIM2s regulates homologous recombination and epithelial-mesenchymal transition. Oncogene 2019;38:2611–26.

28 Balaji K, Vijayaraghavan S, Diao L et al. AXL inhibition suppresses the DNA damage response and sensitizes cells to PARP inhibition in multiple cancers. Mol Cancer Res 2017; **15**: 45–58.

29 Kwak TK, Sohn EJ, Kim S et al. Inhibitory effect of ethanol extract of Ocimum sanctum on osteopontin mediated metastasis of NCI-H460 non-small cell lung cancer cells. BMC Complement Altern Med 2014; **14**: 419.

30 Morra F, Luise C, Visconti R et al. New therapeutic perspectives in CCDC6 deficient lung cancer cells. Int J Cancer 2015; **136**: 2146–57.

31 Qiao GB, Wu YL, Yang XN et al. High-level expression of Rad51 is an independent prognostic marker of survival in non-small-cell lung cancer patients. Br J Cancer 2005; **93**: 137–43.

32 Takenaka T, Yoshino I, Kouso H et al. Combined evaluation of Rad51 and ERCC1 expressions for sensitivity to platinum agents in non-small cell lung cancer. Int J Cancer 2007; **121**: 895–900.